

# A photochemical model for the carbon-rich planet WASP-12b

Ravi kumar Kopparapu<sup>1,2</sup>, James F. Kasting<sup>1,2</sup> and Kevin J. Zahnle<sup>3</sup>

## ABSTRACT

The hot Jupiter WASP-12b is a heavily irradiated exoplanet in a short period orbit around a G0-star with twice the metallicity of the Sun. A recent thermochemical equilibrium analysis based on Spitzer and ground-based infrared observations suggests that the presence of CH<sub>4</sub> in its atmosphere and the lack of H<sub>2</sub>O features can only be explained if the carbon-to-oxygen ratio in the planet's atmosphere is much greater than the solar ratio ( $[C]/[O] = 0.54$ ). Here, we use a 1-D photochemical model to study the effect of disequilibrium chemistry on the observed abundances of H<sub>2</sub>O, CO, CO<sub>2</sub> and CH<sub>4</sub> in the WASP-12b atmosphere. We consider two cases: one with solar  $[C]/[O]$  and another with  $[C]/[O] = 1.08$ . The solar case predicts that H<sub>2</sub>O and CO are more abundant than CO<sub>2</sub> and CH<sub>4</sub>, as expected, whereas the high  $[C]/[O]$  model shows that CO, C<sub>2</sub>H<sub>2</sub> and HCN are more abundant. This indicates that the extra carbon from the high  $[C]/[O]$  model is in hydrocarbon species. H<sub>2</sub>O photolysis is the dominant disequilibrium mechanism that alters the chemistry at higher altitudes in the solar  $[C]/[O]$  case, whereas photodissociation of C<sub>2</sub>H<sub>2</sub> and HCN is significant in the super-solar case. Furthermore, our analysis indicates that  $\zeta h_2$  is the major absorber in the atmosphere of WASP-12b and the absorption features detected near 1.6 and 8 micron may be arising from C<sub>2</sub>H<sub>2</sub> rather than CH<sub>4</sub>. The Hubble Space Telescope's WFC3 can resolve this discrepancy, as  $\zeta h_2$  has absorption between 1.51 – 1.54 microns, while CH<sub>4</sub> does not.

*Subject headings:* stars: planetary systems

## 1. Introduction

The discovery of the first transiting planet, HD 209458b (Charbonneau et al. 2000; Henry et al. 2000), opened up a new window to observe and study extrasolar planetary

---

<sup>1</sup>Department of Geosciences, Penn State University, 443 Deike Building, University Park, PA 16802, USA

<sup>2</sup>Virtual Planetary Laboratory

<sup>3</sup>NASA Ames Research Center, MS 245-3, Moffett Field, CA 94035

systems. By combining transit data with radial velocity measurements, one can determine the mass and radius of a transiting planet (Mazeh et al. 2000; Laughlin et al. 2005a,b; Holman & Murray 2005; Agol et al. 2005). Apart from these physical properties of the planet, it has also been shown that the transmission and emission spectra from ground- and space-based observations can be used to place constraints on the atmospheric composition (Charbonneau et al. 2002; Vidal-Madjar et al. 2003, 2004; Tinetti et al. 2007; Snellen et al. 2008; Swain et al. 2009a,b), brightness temperature (Deming et al. 2005; Charbonneau et al. 2005) and even day-night temperature contrast (Knutson et al. 2007) of transiting planets. To date, most of the planets discovered are “hot Jupiters” (Collier-Cameron 2002), but recently terrestrial mass planets are also being discovered (Léger et al. 2009; Charbonneau et al. 2009).

The observational determination of chemical species that exist in the outer atmospheric layers of transiting planets provides us with an opportunity to investigate the underlying chemistry. Typically, thermochemical equilibrium has been assumed in models of exoplanet atmospheres (Burrows et al. 1997; Fortney et al. 2005; Seager et al. 2005; Marley et al. 2007; Madhusudhan et al. 2011). This is a good assumption at the high temperatures and high pressures prevailing in the lower layers of close-in gas giants. Disequilibrium caused either by the UV flux of the host star (photochemistry) or by eddy and molecular diffusion (vertical transport) have been considered in some models (Liang et al. 2003; Cooper & Showman 2006; Zahnle et al. 2009a,b; Line et al. 2010; Moses et al. 2011). These studies showed that disequilibrium mechanisms can be significant in determining the chemical composition of hot Jupiters.

Here, we investigate the significance of photochemistry and transport in determining the abundances of major species,  $\text{H}_2\text{O}$ ,  $\text{CO}$  and  $\text{CH}_4$ , observed in the dayside thermal emission spectrum (Madhusudhan et al. 2011; Croll et al. 2011) of the transiting hot-Jupiter WASP-12b (Hebb et al. 2009). At the time of its discovery, WASP-12b was the most highly irradiated exoplanet ( $T > 2500$  K) with the largest radius ( $1.79R_J$ ) and the shortest orbital period (1.09 days). Recently, Madhusudhan et al. (2011) reported that Spitzer Space Telescope observations show strong absorption features of  $\text{CH}_4$  in the  $3.6 \mu\text{m}$  channel and  $\text{CO}$  in the  $4.5 \mu\text{m}$  channel, whereas weaker features were observed in the  $5.8 \mu\text{m}$  channel where  $\text{H}_2\text{O}$  absorbs. This suggests that  $\text{CH}_4$  and  $\text{CO}$  are dominant and that  $\text{H}_2\text{O}$  is less abundant in the atmosphere of WASP-12b. Assuming equilibrium chemistry and solar  $[\text{C}]/[\text{O}] = 0.54$ ,  $\text{H}_2\text{O}$  and  $\text{CO}$  should be the dominant species and  $\text{CH}_4$  and  $\text{CO}_2$  should be the least abundant. Therefore, a solar  $[\text{C}]/[\text{O}]$  ratio is ruled out. Madhusudhan et al. (2011) conclude that to explain the observed abundance of  $\text{CH}_4$  and  $\text{CO}$ , WASP-12b must have  $[\text{C}]/[\text{O}] \geq 1$ , implying that it is a carbon-rich planet.

WASP-12b is one of the most highly irradiated known exoplanets, so photochemistry could play an important role in determining its atmospheric composition. Assuming  $[C]/[O] = 1$ , analysis of observations using equilibrium chemistry models suggests mixing ratios (with respect to molecular hydrogen) less than  $10^{-7}$  for  $H_2O$ , greater than  $10^{-4}$  for  $CO$ ,  $\sim 10^{-5}$  for  $CH_4$  and less than  $10^{-9}$  for  $CO_2$ . Our goal in this study is to examine how the vertical distribution and abundances of these species are affected by photochemistry. Specifically, we wish to determine whether photochemical models make qualitatively different predictions from those of thermochemical equilibrium models. We consider two cases, one with solar  $[C]/[O] = 0.54$  and another with  $[C]/[O] = 1.08$ , both of which have also been studied with equilibrium models.

## 2. Model description

We use a one-dimensional photochemical model initially developed to study primitive terrestrial atmospheres (Kasting 1982, 1983; Zahnle 1986; Kasting 1990). The model has been modified to suit the hot Jupiter temperature regime by including "backwards" chemical reactions that do not occur at the low temperatures and pressures encountered in the Earth's atmosphere (Line et al. 2010; Moses et al. 2011). This model solves a set of nonlinear, coupled ordinary differential equations (ODEs) for the mixing ratios of all species at all heights using the reverse Euler method. The method is first order in time and uses second-order centered finite differences in space. We include the following 31 chemical species involved in 230 reactions: O,  $O_2$ ,  $H_2O$ , H, OH,  $CO_2$ , CO, HCO,  $H_2CO$ ,  $CH_4$ ,  $CH_3$ ,  $CH_3O$ ,  $CH_3OH$ , CH,  $CH_2$ ,  $H_2COH$ , C,  $C_2$ ,  $C_2H$ ,  $C_2H_2$ , N,  $N_2$ , NH,  $NH_2$ ,  $NH_3$ , CN, HCN,  $H_2$ , He,  $O(^1D)$  and  $^1CH_2$ . These species are divided into long-lived species (from O to  $H_2$ ), short-lived species ( $O(^1D)$  and  $^1CH_2$ ) and "inert" species (He). Both chemistry and vertical transport by eddy diffusion are considered for long-lived species, whereas transport is neglected for short-lived species. Constant mixing ratios with altitude are assumed for "inert" species. The reaction list and rate constants were obtained from Zahnle (2011) and are listed in Table 1. We have taken only the "forward" reactions and corresponding rate coefficients,  $k_f$ , from Zahnle (2011): The reverse rate coefficients,  $k_r$ , at each temperature level (grid) were calculated assuming thermodynamic-equilibrium:  $k_r = k_f/k_{eq}$ , where  $k_{eq}$  is the equilibrium constant for the reaction and is given by  $k_{eq} = e^{\Delta G^\circ/RT}$ . Here  $\Delta G^\circ$  is the change in the Gibbs free energy for the reaction and is calculated from the Gibbs free energy of formation of reactants and products obtained from NIST-JANAF thermochemical tables when available<sup>1</sup> (and from

---

<sup>1</sup><http://webbook.nist.gov/chemistry/>

NASA thermobuild website<sup>2</sup> when not available):  $\Delta G^\circ = \Delta G_f^\circ(\text{reactants}) - \Delta G_f^\circ(\text{products})$ . However, it should be noted that one cannot simply calculate  $k_r$  as discussed above. This is because the rate coefficients are given in units applicable to number densities whereas the thermodynamic quantities (enthalpy, entropy & Gibbs energies) are calculated at a reference pressure (usually 1 bar). For reactions that have different number of reactants and products, proper pressure terms must be added to obtain accurate rate coefficients. We have appropriately included these terms in our reverse rates. Discussion of these correction terms is given section 2.2 of Visscher & Moses (2011).

As lower boundary conditions, we fix the mixing ratios of the species at thermodynamic equilibrium values. Constant (zero) deposition velocities are assumed for the other species. The upper boundary condition is set to zero flux for all the long-lived species. A more detailed description of the numerical scheme employed in this model is given in Pavlov et al. (2001).

The vertical grid has 100 altitude levels, ranging from 0 km (lower boundary) to 12,800 km (upper boundary) in 128-km increments. The lower boundary pressure is set at 1 bar, and the upper boundary is fixed at  $10^{-8}$  bar. Going to higher pressures is unnecessary, because the species profiles are already close to thermodynamic equilibrium well above the 1-bar level. For the temperature profile, we use one of the best-fit models from Madhusudhan et al. (2011) which has no inversion (purple curve in their Fig. 1). The pressure profile was recalculated from this temperature profile by assuming hydrostatic equilibrium and using the calculated mean molecular weights from the photochemical model. Vertical transport is parameterized as eddy diffusion, as is common in one-dimensional photochemical models. The dayside eddy diffusion profile from Fig. 1 of Line et al. (2010), which is originally obtained from the vertical winds from HD 189733b GCM of Showman et al. (2009), is adopted. We have also performed sensitivity tests by varying eddy profiles, as discussed in §4. Both the temperature and eddy profiles in our photochemical model are shown in Fig. 1.

For comparative purposes, we also calculate the thermodynamic equilibrium mixing ratios for all the species in the photochemical model at each altitude by solving simultaneously a system of chemical equilibrium equations. These equations require the total elemental abundances of carbon, oxygen, hydrogen and nitrogen (as we consider only compounds from these elements) and Gibbs free energies as a function of temperature. Solar elemental abundances from Asplund et al. (2005) are assumed to be our base values, but we report results for both solar  $[C]/[O]$  and  $2 \times$  solar  $[C]/[O]$ . To calculate Gibbs free energies, the enthalpy of formation at the reference temperature (298 K) and entropy are needed. We then use the

---

<sup>2</sup><http://www.grc.nasa.gov/WWW/CEAWeb/ceaThermoBuild.htm>

expressions given in Chase (1998) (p. 16) to calculate Gibbs free energy of formation for each species.

We initially tested our model by attempting to reproduce the results of Line et al. (2010), for the hot Jupiter planet HD189733b. The dayside temperature and eddy diffusion profiles were taken from their Fig. 1. The lower boundary pressure was fixed at 10 bar. Both the thermochemical equilibrium and photochemical model results are shown in Fig. 8 of appendix A and are in good agreement with the similar analyses of Line et al. (2010) and Moses et al. (2011). Moreover, our model maintains equilibrium concentrations for all the major species in the deeper levels ( $\sim 10$  bar), as it should at high temperatures and pressures.

The star WASP-12 is a G0 star<sup>3</sup> with an effective temperature of 6350 K and twice the solar metallicity (Hebb et al. 2009). To simulate its spectrum, we used a G0V star spectrum from Pickles stellar spectral flux library (Pickles 1998)<sup>4</sup>, normalized to a solar flux of  $1360 \text{ W m}^{-2}$  (the value at Earth’s orbit today). We then multiplied the flux at each wavelength by a value consistent with inverse square law of the distance to get the correct flux for WASP-12b. The Pickles spectra are normalized to 1 at  $5556\text{\AA}$ . The fluxes from this dimensionless model spectrum are converted to  $\text{W m}^{-2}\text{nm}^{-1}$  by multiplying the following flux expression from Gray (1992):

$$\log F_{5556} = -0.40V - 8.449 \quad (1)$$

where  $F_{5556}$  is the flux at  $5556\text{\AA}$  and  $V$  is the visual magnitude of the star. For WASP-12,  $V = 11.69$  (Hebb et al. 2009). In Fig. 2, we show the G0V star spectrum along with F2V and the Sun. A fixed stellar zenith angle of  $50^\circ$  is assumed in all our models, the same value that is used in our models of Earth’s atmosphere (e.g. Pavlov et al. (2001)). This value is close to the value of  $48^\circ$  used by Moses et al. (2011) to reproduce secondary transit spectra in the atmosphere of HD 189733b.

### 3. Results

We consider two different cases. In the first, we assume  $[\text{C}]/[\text{O}] = 0.54$  (solar), and in the second we assume  $[\text{C}]/[\text{O}] = 1.08$  (twice solar). Fig. 3 shows mixing ratio profiles of some of the major species in our model, plotted against pressure for solar  $[\text{C}]/[\text{O}]$  abundance. The lower boundary in both the models is kept at 1 bar pressure ( $T = 2841 \text{ K}$ ) as

---

<sup>3</sup>[http://www.superwasp.org/wasp\\_planets.htm](http://www.superwasp.org/wasp_planets.htm)

<sup>4</sup><http://cdsarc.u-strasbg.fr/viz-bin/Cat?J/PASP/110/863>

the observed spectral features mostly arise from pressures equal to or less than the 1-bar level (Fortney et al. 2005; Tinetti et al. 2007; Swain et al. 2009a; Madhusudhan et al. 2011). Dashed lines represent the profile obtained from equilibrium chemistry, solid lines from our photochemical model and filled squares represent mixing-ratios of respective species at the lower boundary.

In the case of solar  $[C]/[O]$  (Fig. 3), most of the oxygen and carbon is in  $H_2O$  and  $CO$ . The chemical loss time scale ( $\tau_{chem}$ ) for  $H_2O$ ,  $CO$  and  $CO_2$  is smaller than the transport time scale ( $\tau_{trans}$ ); hence, as altitude increases the abundances stay at their equilibrium values until  $\sim 10^{-5}$  bar (Prinn & Barshay 1977). Below this pressure level (i.e., at higher altitudes)  $H_2O$  gets photolyzed.  $H_2O$  photolyzes at lower altitudes than does  $CO$  because the dissociation energy for  $H_2O$  (5.17 eV) is lower than that of  $CO$  (11.14 eV) (Yung & DeMore (1999), Table 2.4). To break this strong C-O bond, photons of wavelength  $\leq 111.3$  nm are needed ( $H_2O$  needs photons of wavelength  $\lesssim 239.8$  to break its bond).  $CO$  photolysis is not simulated in our photochemical model and it can be a source of carbon and oxygen photochemistry at high altitudes (Line et al. 2010; Moses et al. 2011), but it should be relatively slow because of the small number of photons at these short wavelengths. By contrast, the photon flux is quite high at the longer wavelengths that can photolyze  $H_2O$  (green curve in Fig. 2 inset).

In the case of  $CO_2$ , the equilibrium abundance is maintained until  $10^{-5}$  bar and is set by the following kinetic reactions that transfer oxygen from  $CO$  and  $H_2O$  to  $CO_2$ :



At altitudes above  $10^{-5}$  bar,  $H_2O$  photolysis becomes the dominant source of  $OH$  production. The  $OH$  then combines with  $CO$  through Eq. (3) to produce excess  $CO_2$  (local maximum of solid light-blue curve  $> 10^{-5}$  bar). Above this level,  $CO_2$  becomes less abundant because it is itself photolyzed.

The shape of the equilibrium profile for  $CH_4$  can be understood from the following reaction



and the corresponding equilibrium constant:

$$K_{eq} = \frac{p_{CH_4} p_{H_2O}}{p_{CO} p_{H_2}^3} \quad (5)$$

where ‘ $p_i$ ’ represents the partial pressure of species  $i$ . The partial pressure is related to the total pressure and volume mixing ratio as  $p_i = f_i \cdot P$ . As pressure increases (going

downward) from  $10^{-8}$  bar, the denominator term on the right-hand side of Eq.(5) increases. Temperature is constant in this region (see Fig. 1), as is the  $\text{H}_2\text{O}/\text{CO}$  ratio. Thus, in order to maintain equilibrium  $\text{CH}_4$  must increase with depth. Below  $10^{-2}$  bar, the temperature starts to increase with depth.  $\text{CH}_4$  is more stable at lower temperatures and is also more sensitive to temperature changes than other species. Hence, it becomes less abundant in the  $10^{-2} - 10^{-1}$  bar regime. At pressures above  $10^{-1}$  bar, the temperature again remains constant, so  $\text{CH}_4$  must again increase with depth as it does in the upper atmosphere.

The  $\text{CH}_4$  profile from the photochemical model (solid magenta curve in Fig. 3) follows the equilibrium profile at pressures up to  $\approx 10^{-2}$  bar. Above this level,  $\tau_{\text{chem}} \sim \tau_{\text{trans}}$  (quench level) and  $\text{CH}_4$  remains well mixed near its equilibrium value of  $10^{-10}$ . Photolysis of  $\text{CH}_4$  occurs above  $10^{-3}$  bar (see Fig.7) mainly through the following reactions:



Although H is produced through  $\text{CH}_4$  photolysis, it is not enough to explain the increase in H abundance between  $10^{-2} - 10^{-3}$  bar (light-blue solid curve in Fig.3). This increase in H is mainly due to the production of OH through  $\text{H}_2\text{O}$  photolysis at this level, which then combines with the most abundant molecule in this atmosphere,  $\text{H}_2$ , through the reverse of reaction (2).



As the OH abundance increases, more  $\text{H}_2$  is consumed and its mixing ratio decreases above  $10^{-5}$  bar (solid black curve in Fig. 3). Eventually,  $\text{H}_2\text{O}$  itself becomes depleted by photolysis, so the production of OH radical diminishes. At this point,  $\text{H}_2$  asymptotically reaches a mixing ratio of  $10^{-2}$ . The increase in H also affects the atomic oxygen abundance (black solid curve in Fig. 3) by the following reaction:



Note that CO photolysis, which is not included in our model, may dominate the above reaction in producing atomic oxygen.

Our analysis shows that, in the  $[\text{C}]/[\text{O}] = 0.54$  case, the abundances of major species (Fig. 3) in WASP-12b’s atmosphere are mainly determined by thermochemical equilibrium, with departures at high altitudes due to disequilibrium chemistry driven by  $\text{H}_2\text{O}$  photolysis.

This is not surprising considering that  $\text{H}_2\text{O}$  is far more abundant than  $\text{CH}_4$ . The photolysis rates of  $\text{H}_2\text{O}$  and  $\text{CH}_4$  as a function of pressure (altitude) for solar (blue) and super-solar (red)  $[\text{C}]/[\text{O}]$  are shown in Fig. 7. In the solar case, at any given height,  $\text{H}_2\text{O}$  is more rapidly photodissociated than is  $\text{CH}_4$ , as it is more abundant. In the super-solar  $[\text{C}]/[\text{O}]$  case (Fig. 4),  $\text{H}_2$  is more abundant than either  $\text{H}_2\text{O}$  or  $\text{CH}_4$ , and so it is photolyzed more rapidly at high altitudes.

Madhusudhan et al. (2011) report that the spectrum obtained from the dayside multi-wavelength photometry of WASP-12b is best explained if one assumes  $[\text{C}]/[\text{O}] \geq 1$ , using chemical equilibrium models. Under this assumption, the atmosphere is depleted in  $\text{H}_2\text{O}$ , enhanced in  $\text{CH}_4$ , and rich in  $\text{CO}$ . These equilibrium model profiles (dashed lines), along with our photochemical model results, for  $[\text{C}]/[\text{O}] = 1.08$  are shown in Fig. 4. In contrast to solar  $[\text{C}]/[\text{O}]$  model, most of the oxygen is now in  $\text{CO}$  (blue solid line), and  $\text{CH}_4$  (magenta curve) is more abundant than  $\text{H}_2\text{O}$  (red curve). The switchover from an atmosphere where  $\text{H}_2\text{O}$  and  $\text{CO}$  are the dominant species to one in which  $\text{CH}_4$  and  $\text{CO}$  become abundant happens precisely at  $[\text{C}]/[\text{O}] = 1$ . This transition is illustrated in Fig. 6.

In Fig. 4 the abundance of  $\text{H}_2\text{O}$  follows the equilibrium profile at pressures up to about  $10^{-2}$  bar in the  $[\text{C}]/[\text{O}] = 1.08$  model. At that point, transport by eddy diffusion becomes faster than the chemical reaction timescale, so the equilibrium value is maintained until  $\sim 10^{-4}$  bar. Photolysis begins above this level, and the abundance of  $\text{H}_2\text{O}$  decreases. The behavior of  $\text{CH}_4$  is similar to the solar  $[\text{C}]/[\text{O}]$  case, though it is relatively more abundant in this high  $[\text{C}]/[\text{O}]$  model. Note that for  $\text{CH}_4$  and  $\text{H}_2\text{O}$ , the photochemical mixing ratios are not exactly equal to the equilibrium values below 0.1 bar. The reason is as follows: At high altitudes (above  $10^{-6}$  bar), atomic hydrogen (green solid curve in Fig. 4) becomes a dominant species (more than  $\text{H}_2$ ). Our photochemical model uses a minor constituent approximation for the diffusion coefficient in a binary mixture (Eq.(15.29), Banks & Kockarts (1973)), which clearly is not applicable to H at this level. Due to this approximation, the mixing ratio of H exceeds unity above  $10^{-6}$  bar, which is unphysical. Therefore, we renormalize the mixing ratios of each species in our photochemical model so that they sum to unity, and hence the equilibrium and photochemical profiles deviate slightly in the lower atmosphere. Note that this should not affect our conclusions in any way regarding which species are dominant (discussed in the next paragraph) in Wasp-12b’s high  $[\text{C}]/[\text{O}]$  model.

As can be seen from Fig. 4, and also pointed by Moses et al. (2011b), the dominant hydrogen species (apart from H and  $\text{H}_2$ ) in this model are HCN and  $\text{H}_2$ . Therefore, the photolysis of these two species drive the disequilibrium chemistry in the upper atmosphere. For example, in the solar model, the catalytic  $\text{H}_2$  destruction mechanism initiated by  $\text{H}_2\text{O}$  photolysis (Eqs. (9) & (10)) was used to explain the increase in H abundance shown in Fig.



3 (green solid curve). A similar increase of H at high altitudes can be noticed in the high [C]/[O] case. Reactions (9) and (10) require OH production through H<sub>2</sub>O photolysis, which is negligible in the high [C]/[O] model. Instead, the following reactions are important:



The results of these reactions can be seen in Fig. 4: At altitudes above  $\sim 10^{-2}$  bar, the photolysis of C<sub>2</sub>H<sub>2</sub> and HCN produce C<sub>2</sub>H, CN and H through the above reactions. An increase in H can be seen as a result. The abundances of CN & C<sub>2</sub>H are not large enough below  $10^{-5}$  bar to have a significant effect on the mixing ratio of H<sub>2</sub>. Above this level, reactions (13) & (15) result in the decrease of H<sub>2</sub> mixing ratio (solid black line in Fig. 4) and corresponding increase of H. Further up, C<sub>2</sub>H<sub>2</sub> and HCN become scarce and the production of C<sub>2</sub>H and CN diminishes, which in turn reduces the rate of production of H. Therefore, H assumes a nearly constant mixing ratio thereafter.

Based on their thermodynamic equilibrium calculations, Madhusudhan et al. (2011) concluded that Wasp-12b is abundant in CH<sub>4</sub> and deficient in H<sub>2</sub>O. Our analysis indicates that both the equilibrium and photochemical models predict C<sub>2</sub>H<sub>2</sub> and HCN are more abundant than CH<sub>4</sub>. Also, C<sub>2</sub>H<sub>2</sub> has strong absorption in the range 2.98 – 3.1 microns and also between 7.2 – 7.9 microns, whereas CH<sub>4</sub> has absorption features between 3.2 – 3.45 microns and 7.3 – 8 microns. The short wavelength range for C<sub>2</sub>H<sub>2</sub> has little overlap with the Spitzer 3.6 micron channel<sup>5</sup> but the longer wavelength range for both species overlaps with Spitzer’s 8 micron channel<sup>6</sup>. In order to determine which is the dominant absorber, we have calculated the optical depths of the C<sub>2</sub>H<sub>2</sub> 7.5 micron band and the CH<sub>4</sub> 7.7 micron band as a function of pressure, as shown in Fig.5. Approximate band-averaged absorption coefficients for these features are  $2 \times 10^{-19}$  cm<sup>2</sup> and  $4 \times 10^{-19}$  cm<sup>2</sup>, respectively<sup>7</sup>. The column depths are taken from our photochemical model. Clearly, C<sub>2</sub>H<sub>2</sub> has a larger optical depth than CH<sub>4</sub> and is the dominant absorber. Note that, Madhusudhan et al. (2011) point out that 0.01 – 1 bar pressure levels contributes most to the observed spectrum and that C<sub>2</sub>H<sub>2</sub> is considerably

---

<sup>5</sup>Band pass range from 3.08–4.01 micron: <http://irsa.ipac.caltech.edu/data/SPITZER/docs/irac/calibrationfil>

<sup>6</sup>Band pass range from 6.15–10.49 microns: <http://irsa.ipac.caltech.edu/data/SPITZER/docs/irac/calibrationf>

<sup>7</sup><http://vpl.astro.washington.edu/spectra/c2h2pnnlimagesmicrons.htm>

more abundant than  $\text{CH}_4$  within this pressure range (Fig. 4). Therefore, future analysis of observations of carbon rich planets (including further analysis of WASP-12b) should consider higher-hydrocarbon species.

## 4. Discussion

Our analysis confirms the previous thermodynamic equilibrium result that a  $[\text{C}]/[\text{O}] \geq 1$  is needed to explain the observed overabundance of  $\text{CH}_4$  in the atmosphere of WASP-12b. A similar conclusion was reached by Line et al. (2010) but for a different hot Jupiter planet, HD 189733b. These authors varied  $[\text{C}]/[\text{O}]$  from 0.1 to 10 times the solar value, while keeping the total metallicity at the solar value (Fig. 6 in their paper), and examined the effect on thermochemical equilibrium mixing ratios at the lower boundary. As  $[\text{C}]/[\text{O}]$  increases, most of the carbon in their model is in CO and  $\text{CH}_4$ . At  $[\text{C}]/[\text{O}] = 1$ ,  $\text{H}_2\text{O}$  and  $\text{CH}_4$  switch their profiles just as they do in our equilibrium models of WASP-12b (Fig. 6). Although our equilibrium models agree qualitatively with theirs, the respective mixing ratios of the major species differ because of different elemental abundances and overall hotter temperatures (their  $\sim 1500$  K versus our 2800 K)

We have also performed a sensitivity test to eddy diffusion varying by 3 orders of magnitude above and below our eddy profile. For the larger case the species concentrations are well mixed over much of the atmosphere, deviating from the equilibrium even at relatively low altitudes ( $\sim 0.1$  bar). Consequently, the photolysis of  $\text{H}_2$  and HCN is not effective in producing atomic hydrogen (as mixing dominates photolysis even at high altitudes). On the other hand, if the eddy diffusion coefficient is small (as proposed by Youdin & Mitchell (2010)), mixing is not effective and photochemistry becomes important at mid altitudes ( $10^{-3} - 10^{-4}$  bar). Therefore, significant deviations from equilibrium occur at all altitudes above this level.

### 4.1. A possible mechanism for the origin of excess carbon in WASP-12b

The high  $[\text{C}]/[\text{O}]$  ratio in WASP-12b is unexpected, considering that the host star has a solar  $[\text{C}]/[\text{O}]$  ratio (see Fossati et al. (2010b) Table 2). In the standard core accretion model (Pollack et al. 1996), volatiles such as carbon and oxygen are expected to remain unfractionated in forming giant planets (Owen et al. 1999). Lodders (2004) pointed out that *Galileo* probe measurements of Jupiter’s atmosphere show an enriched carbon abundance of 1.7 times solar and a depletion of oxygen by a factor of 4 (but see further discussion below).

To explain this result, Lodders (2004) proposed a model in which carbonaceous matter began to condense in the solar nebula beyond 5 AU, thereby providing the increased mass density needed for rapid core growth. By contrast, in the standard accretion model, Jupiter forms just beyond the “ice line” where water ice begins to condense. In the Lodders (2004) model, the ice line would have been farther out, beyond the orbit of Jupiter, and this would explain Jupiter’s apparent deficiency in O relative to C. A similar mechanism might then account for the high [C]/[O] ratio in WASP 12b.

Although the Lodders (2004) model could be correct, we suspect that Jupiter formed beyond the ice line, with a solar [C]/[O] ratio, and that other factors are responsible for observed [C]/[O] enrichments in exoplanets. The Galileo Probe is widely thought to have descended into an infrared “hot spot” (Atreya et al. 1999), that is, an area of downwelling air that had been depleted in H<sub>2</sub>O during its uplift from below. In support of this idea, the H<sub>2</sub>O mixing ratio was observed to gradually increase with depth down to 20 bars, at which point the probe lost contact with Earth (see Atreya et al. (1999) Table 1). Furthermore, thunderstorms and lightning were also observed by the probe deeper than 4 – 5 bars (Gierasch et al. 2000; Ingersoll et al. 2000; Atreya et al. 2005), which is consistent with equilibrium cloud condensatation models which predict that water clouds can form in this pressure range if the oxygen abundance is at least solar (Atreya et al. 2005)<sup>8</sup>.

As an alternative to the Lodders (2004) model, we suggest that the high [C]/[O] for WASP-12b arose because the primordial disk was depleted in oxygen abundance during the giant planet’s migration. The carbon compounds (CH<sub>4</sub>, CO) may have been trapped in ices in the form of planetesimals and then accreted onto the envelope of the gas giant, resulting in the observed enhancement of [C]/[O] > 1. Assuming that the disk started with solar elemental abundances of carbon ( $2.26 \times 10^{-4}$ ) and oxygen ( $4.20 \times 10^{-4}$ ), in order to obtain [C]/[O] = 1.08 in WASP-12b (our high [C]/[O] model case), the [O] abundance in the disk must have been depleted by  $\approx 50\%$ . Recently, Madhusudhan et al. (2011b) performed a more detailed analysis of the formation of WASP-12b and concluded that the primordial disk was depleted in [O] by 41%. The discrepancy in our numbers arises because Madhusudhan et al. (2011b) used elemental abundances of the host star WASP-12 (Fossati et al. 2010b), which are  $3.54 \times 10^{-4}$  and  $7.94 \times 10^{-4}$  for [C] & [O], respectively.

It is possible that the depletion of [O] in WASP-12b occurred because the host star accreted fractionated refractory materials (that trapped 41% of [O], in the WASP-12 case)

---

<sup>8</sup>It should be noted that, because the base level of the water clouds was not determined, the water abundance in the deep well-mixed regions of Jupiter is still unknown. However, this does not change the observed result that the mixing ratio of H<sub>2</sub>O gradually increases with depth.

from the protoplanetary disk during planetary formation. In our Solar System, planetary migration could have affected giant planet composition to some extent, as Jupiter and Saturn, in particular, are thought to have moved around considerably during planetary accretion (Tsiganis et al. 2005; Gomes et al. 2005; Morbidelli et al. 2005; Walsh et al. 2011), with Jupiter perhaps coming as close in as 1.5 AU. But, as far as we know, giant planets never migrated through the terrestrial planet region of our system. By contrast, in the WASP-12 system, planetary migration was evidently much more pronounced. WASP-12b migrated from the outer parts of the nebula to its present location close to the star. Meanwhile, rocky planets formed in the hot, inner parts of the nebula may have migrated in even closer and been consumed by the star. If WASP-12b accreted additional material during its journey, that material would have been depleted in O relative to C, possibly accounting for the high  $[C]/[O]$  ratio of the planet. Madhusudhan et al. (2011b) mention this possibility, but they rule it out because they argue this would require that  $[C]/[H]$  in the envelope of WASP-12b should be close to the host star’s value, which is not the case. We don’t agree with this objection, however, because all known planets accrete elements heavier than He more efficiently than they do H. Jupiter, for example, is enriched in C, N, and S compared to the Sun by a factor of 3 (Beatty 1999). Further observations may be needed to determine the validity of this mechanism.

The accretion of refractory elements onto a star has been proposed as one of the reasons why solar twins and analogs in the solar neighborhood have enhanced heavy elemental abundances compared to the Sun (Meléndez et al. 2009; Ramírez et al. 2009). These studies found that the abundances of heavy elements in these solar analog stars increase with their condensation temperature. The authors attribute the apparent depletion of refractory elements in the Sun to the existence of terrestrial planets, and they suggest that Sun accreted refractory-depleted material from the nebula during the formation of the solar system<sup>9</sup>. Indeed, Chambers (2010) showed that adding  $4 M_{\oplus}$  of Earth-like and carbonaceous-chondrite-like material to the solar convection zone brings the Sun’s elemental abundance in line with the mean abundances of solar twins.

Recently, Schuler et al. (2011) derived precise elemental abundances for ten stars using high-resolution spectroscopy. All ten of their stars have at least one giant planet around them at different orbital distances. Their analysis indicated that four stars, all of which have hot Jupiters ( $\sim 0.05$  AU), show positive correlations between refractory elemental abundance and condensation temperature. This implies that these stars may have accreted refractory-rich planetary material or cores. If a similar accretion happened during the formation of

---

<sup>9</sup>Note that the accreted material is not depleted in elements such as carbon because they have low condensation temperatures and so did not condense in the inner part of the solar nebula.

the WASP-12 system, then “pollution” signatures in the atmosphere of WASP-12 may be observable. Formation models of protostars from molecular clouds (Wuchterl & Tscharnuter 2003) indicate that solar-mass protostars have thin convective envelopes ( $\sim 0.02 M_{\odot}$ ), similar to the present day Sun, and hence mixing of deposited material may not be significant. But it has been suggested that WASP-12b may be losing mass to its star (Li et al. 2010). If this is the case, then it could be difficult to determine how much of the refractory material has accreted onto WASP-12 during its formation. Fossati et al. (2010b) performed a detailed spectropolarimetric analysis of WASP-12 to look for pollution signatures due to the material lost by WASP-12b. They found hints of pollution but were unable to draw firm conclusions. A differential analysis of WASP-12 twins (with the same effective temperature, age and metallicity), identifying their abundances with high precision, is required to determine if the refractory elemental abundance of WASP-12 does indeed increase with condensation temperature.

## 5. Conclusions

In this study, we analyzed how a disequilibrium mechanism such as photochemistry can affect the observed abundances of  $H_2O$ ,  $CO$ ,  $CO_2$  and  $CH_4$  in the WASP-12b atmosphere. We considered two models, with  $[C]/[O] = 0.54$  (solar) and  $[C]/[O] = 1.08$  (twice solar). Although our photochemical results agree that high  $[C]/[O]$  is needed to explain the observed high abundance of  $CH_4$  and lack of observable  $H_2O$ , they also indicate  $2h2$  and  $HCN$  are more abundant than  $CH_4$  and should be taken into consideration in modeling hot-jupiter atmospheres<sup>10</sup>. More importantly, our results indicate that  $2h2$  is the dominant absorber at 1.6 and 8 micron in WASP-12b’s atmosphere and the absorption features may possibly be arising from  $2h2$  rather than  $CH_4$ . Observations with Hubble Space Telescope’s WFC3 can resolve this discrepancy.

We also propose a possible mechanism for the origin of the excess carbon observed in WASP-12b. Following other authors, we suggest that WASP-12 may have accreted rocky, O-rich material from the nebula during the formation of the system, leaving the disk relatively enriched in other volatiles such as C and N. WASP-12b then accreted some of this high  $[C]/[O]$  material, which thereby gave rise to the high  $[C]/[O]$  ratio of the planet. Testing this hypothesis requires that we understand whether WASP-12 is currently stealing mass from its planet, WASP-12b. A high precision abundance analysis of WASP-12 twins and analogs

---

<sup>10</sup>Note that this prediction is not specifically a result of our photochemical model, as our thermodynamic equilibrium models predict this, as well.

can shed light on the refractory elemental abundance of WASP-12 and the possible origin of excess carbon in WASP-12b.

The authors would like to thank the referee, Julianne Moses, for pointing to us the importance of  $\text{ZrH}_2$  and HCN chemistry and for her in-depth analysis of our work which helped in improved photochemical models and our current manuscript. R. K and J.F.K gratefully acknowledge funding from NASA Astrobiology Institute's Virtual Planetary Laboratory lead team, supported by NASA under cooperative agreement NNH05ZDA001C, and the Penn State Astrobiology Research Center.

## REFERENCES

- Agol, E., Steffen, J.; Sari, R.; & Clarkson, W. 2005, MNRAS, 359, 567
- Asplund, M., Grevesse, N. & Sauval, A. in. Cosmic Abundances as Records of Stellar Evolution and Nucleosynthesis (eds Barnes, T. G. III & Bash, F. N.) 2538 (ASP Conf. Ser. 336, 2005).
- Atreya, S. K. et al. 1999, Planetary & Space Science, 47, 1243
- Atreya, S. K., & Wong, A. 2005, Space Science reviews, 116, 121
- Banks, P. M., & Kockarts, G. 1973, Aeronomy, Academic Press Inc. New York
- Beatty, J. K. 1999, *The New Solar System*, Cambridge University Press, Massachusetts
- Burrows, A., et al. 1997, ApJ, 491, 856
- Chambers. J. E. 2010, ApJ, 724, 92
- Charbonneau, D., Brown, T.M., Latham, D.W., & Mayor, M. 2000, ApJ, 529, L45
- Charbonneau, D., Brown, T.M., Noyes, R.W., & Gilliland, R.L. 2002, ApJ, 568, 377
- Charbonneau, D., et al. 2005, ApJ, 626, 523
- Charbonneau, D., et al. 2009, Nature, 462, 891
- Chase, M. W., Jr., 1998, NIST-JANAF Thermochemical Tables, Fourth Edition, J. Phys. Chem. Ref. Data.
- Collier-Cameron, A. 2002, Astron. Geophys., 43, 421

- Cooper, C. S., & Showman, A. P. 2006, *ApJ*, 649, 1048
- Croll, B., et al. 2011, *AJ*, 141, 30
- Deming, D., Seager, S., Richardson, L.J. & Harrington, J. 2005, *Nature*, 434, 740
- Fortney, J. J., Marley, M. S., Lodders, K., Saumon, D., & Freedman, R. 2005, *ApJ*, 627, 69
- Fossati, L. et al. 2010b, *ApJ*, 720, 872
- Gray, D., 1992, *The Observation and Analysis of Stellar Photospheres*, 2nd edn., Cambridge University Press, Cambridge.
- Gierasch, P. J. et al. 2000, *Nature*, 403, 628
- Gomes, R., Levison, H. F., Tsiganis, K., & Morbidelli, A. 2005, *Nature*, 435, 466
- Hebb, L. et al. 2009, *ApJ*, 693, 1920
- Henry, G. W., Marcy, G. W., Butler, R. P., & Vogt, S. S. 2000, *ApJ*, 529, L41
- Holman, M. J., & Murray, N. W. 2005, *Science*, 307, 1288
- Ingersoll, A. P. et al. 2000, *Science*, 403, 630
- Kasting, J. F., 1982, *J. Geophys. Res.*, 87, 3091
- Kasting, J. F. et al., 1983, *Precambrian Res.*, 20, 121
- Kasting, J.F., 1990, *Origins of Life Evol. Biosphere*, 20, 199
- Kasting, J. F. 2010, *How to find a Habitable Planet*, Princeton University Press
- Kuntson, H. A., et al. 2007, *Nature*, 447, 183
- Laughlin, G., Marcy, G. W., Vogt, S. S., Fischer, D. A., & Butler, R. P. 2005a, *ApJ*, 629, L121
- Laughlin, G., Wolf, A., Vanmunster, T., Bodenheimer, P., Fischer, D., Marcy, G., Butler, P., & Vogt, S. 2005b, *ApJ*, 621, 1072
- Léger et al. 2009, *A&A*, 506, 287
- Lewis, J. S. 1974, *Science*, 186, 440
- Li, S. et al., 2010, *Nature*, 463, 1054

- Liang, M. C., Parkinson, C. D., Lee, A. Y.-T., Yung, Y. L., & Seager, S. 2003, *ApJ*, 596, L247
- Line, M. R., et al. 2010, *ApJ*, 717, 496
- Lodders, K. 2003, *ApJ*, 591, 1220
- Lodders, K. 2004, *ApJ*, 611, 587
- Madhusudhan, N. et al. 2011, *Nature*, 469, 64
- Madhusudhan, N. et al. 2011b, arXiv:1109.3183
- Marley, M. S., Fortney, J. J., Hubickyj, O., Bodenheimer, P., & Lissauer, J. J. 2007, *ApJ*, 655, 541
- Mazeh, T., et al. 2000, *ApJ*, 532, L55
- Meléndez, J., et al. 2009, *ApJ*, 704, L66
- Morbidelli, A., Levison, H. F., Tsiganis, K., & Gomes, R. 2005, *Nature*, 435, 462
- Moses, J. I., et al. 2011, submitted, arXiv:1102.0063
- Moses, J. 2011, private communication
- Owen, T., et al. 1999, *Nature*, 402, 269
- Pavlov, A., Brown, L., & Kasting, J. F. 2001, *J. Geophys. Res.*, 106, 23267
- Pickles, A. J., 1998, *PASP*, 110, 863
- Pollack, J. B., et al. 1996, *Icarus*, 124, 62
- Prinn, R. G., & Barshay, S. S. 1977, *Science*, 198, 1031
- Ramírez, I., et al. 2009, *A&A*, 508, L17
- Schuler, S. C., et al. 2011, arXiv:1103.0757
- Seager, S., et al. 2005, *ApJ*, 632, 1122
- Showman, A. P., et al. 2009, *ApJ*, 699, 564
- Snellen, I.A.G., Albrecht, S., de Mooij, E.J.W., & Le Poole, R.S. 2008, *A&A*, 487, 357



- Swain, M. R., Vasisht, G., Tinetti, G., Bouwman, J., Chen, P., Yung, Y., Deming, D., & Deroo, P. 2009a, *ApJ*, 690, L114
- Swain, M. R., et al. 2009b, *ApJ*, 704, 1616
- Tinetti, G., et al. 2007, *Nature*, 448, 169
- Tsiganis, K., Gomes, R., Morbidelli, A., & Levison, H. F. 2005, *Nature*, 435, 459
- Vidal-Madjar, A., Lecavelier des Etangs, A., Désert, J.-M., Ballester, G. E., Ferlet, R., Hebrard, G., & Mayor, M. 2003, *Nature*, 422, 143
- Vidal-Madjar, A., et al. 2004, *ApJ*, 604, L69
- Visscher, C., & Moses, J. 2011, *ApJ*, 738, Issue 1, article id. 72
- Walsh, K. J., et al. 2011. *Nature*, 475, 206
- Wuchterl, G., & Tscharnuter, W. M. 2003, *A&A*, 398, 1081
- Youdin, A. N., & Mitchell, J. L. 2010, *ApJ*, 721, 1113
- Yung, L. Y., & DeMore, W. B. 1999, *Photochemistry of Planetary Atmospheres*, Oxford University Press
- Zahnle, K., 1986, *J. Geophys. Res.*, 91, 2819
- Zahnle, K., Marley, M. S., & Fortney, J. J. 2009a, arXiv:0911.0728
- Zahnle, K., Marley, M. S., Freedman, R. S., Lodders, K., & Fortney, J. J. 2009b, *ApJ*, 701, L20
- Zahnle, K. 2010, Private communication. Reaction list provided in the online version of the *Journal*

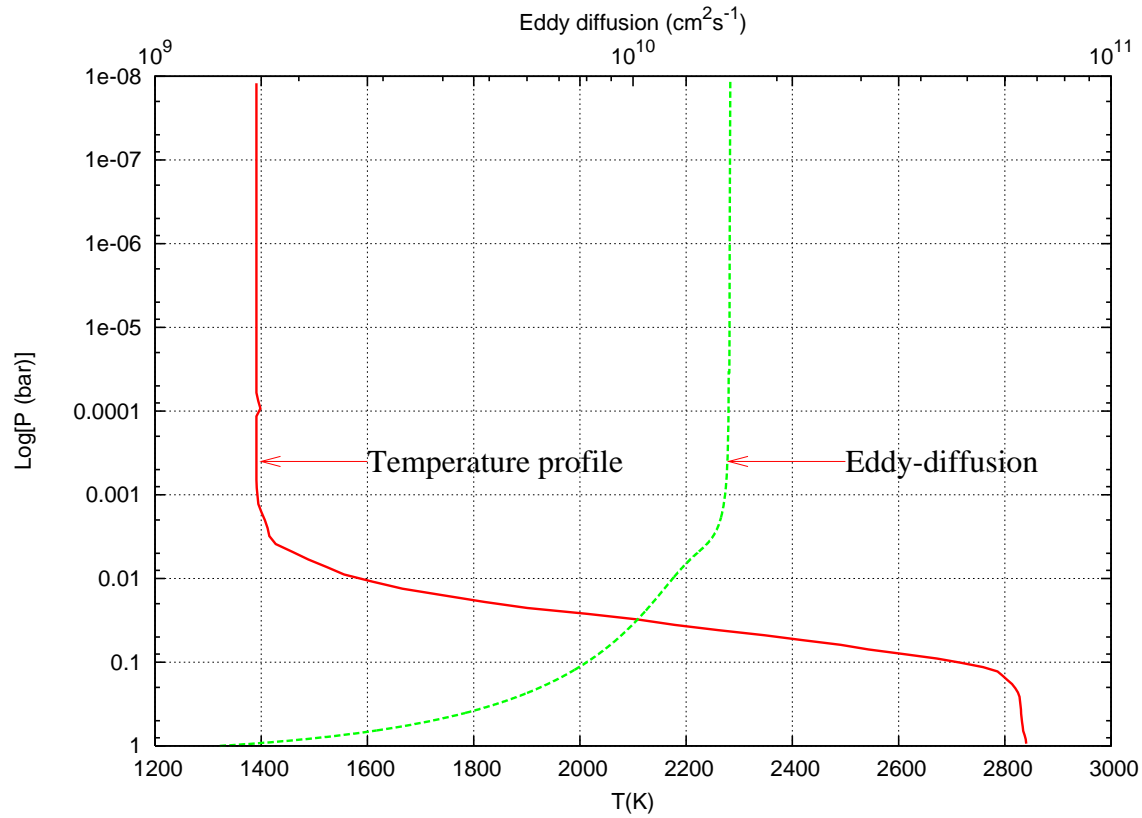


Fig. 1.— Temperature profile (red solid curve) and eddy diffusion profile (green dashed line) used in our photochemical model. The temperature profile is taken from one of the models of Madhusudhan et al. (2011) with no inversion, as a profile with inversion is ruled out by the data. This profile is then recalculated using hydrostatic equilibrium to be consistent with our photochemical model. Eddy diffusion profile is taken from the dayside profile of Line et al. (2010).

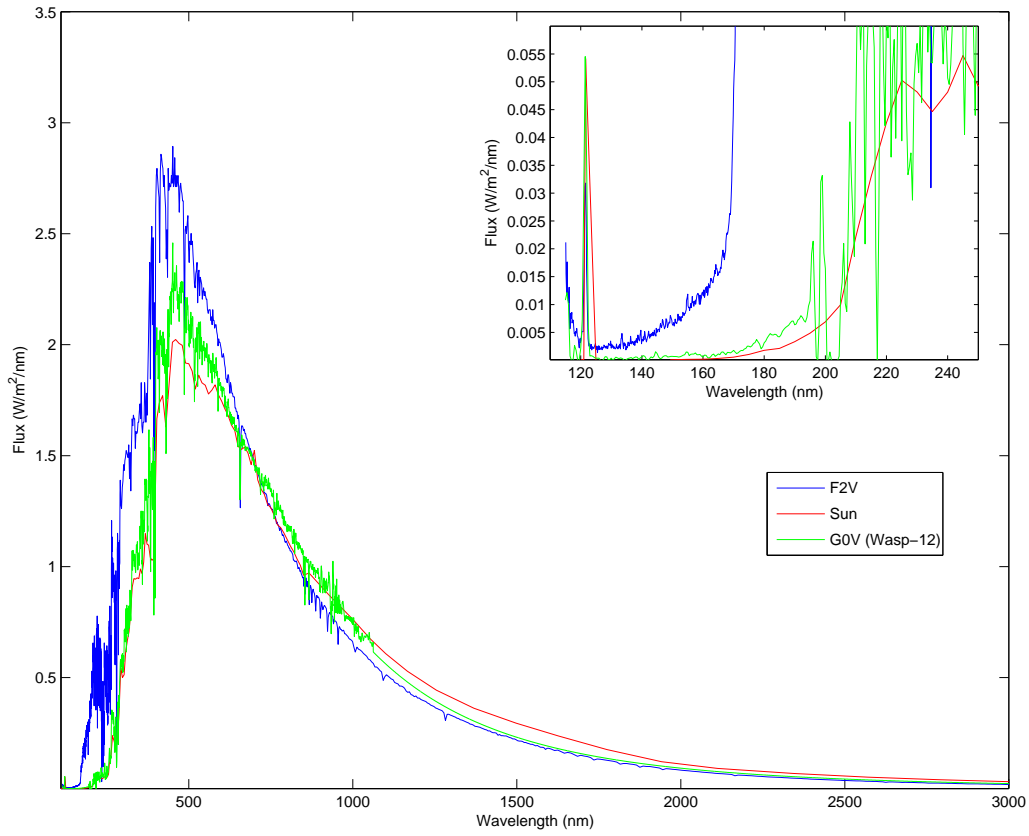


Fig. 2.— Comparison of the normalized flux of a G0V stellar spectrum from Pickles (1998) stellar flux library (green curve), which is assumed for the star WASP-12, with an F2V star (top blue curve) and the Sun (red bottom curve). Inset figure shows the UV region.

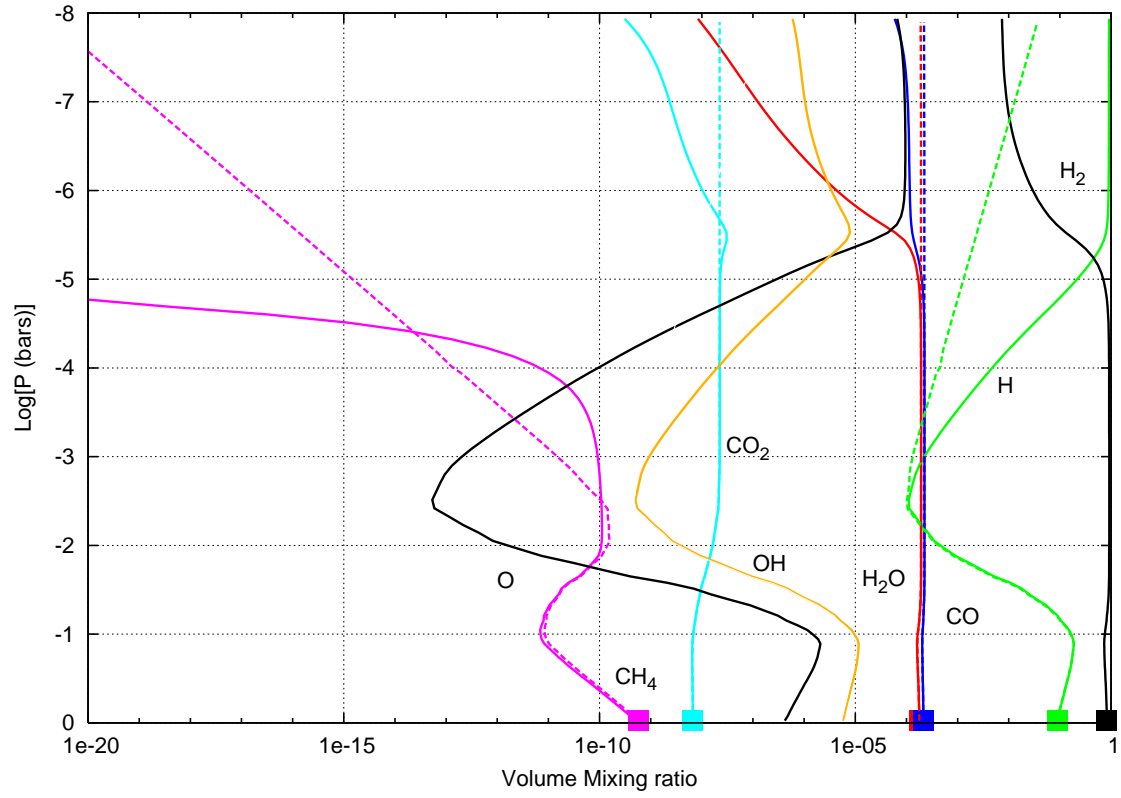


Fig. 3.— Equilibrium (dashed) and photochemical (solid) mixing ratio profiles of major species, for  $[C]/[O] = 0.54$  (the solar value). Filled squares represent equilibrium values at the lower boundary. The mixing ratios refer to volume mixing ratio. The Helium abundance is 0.07836.

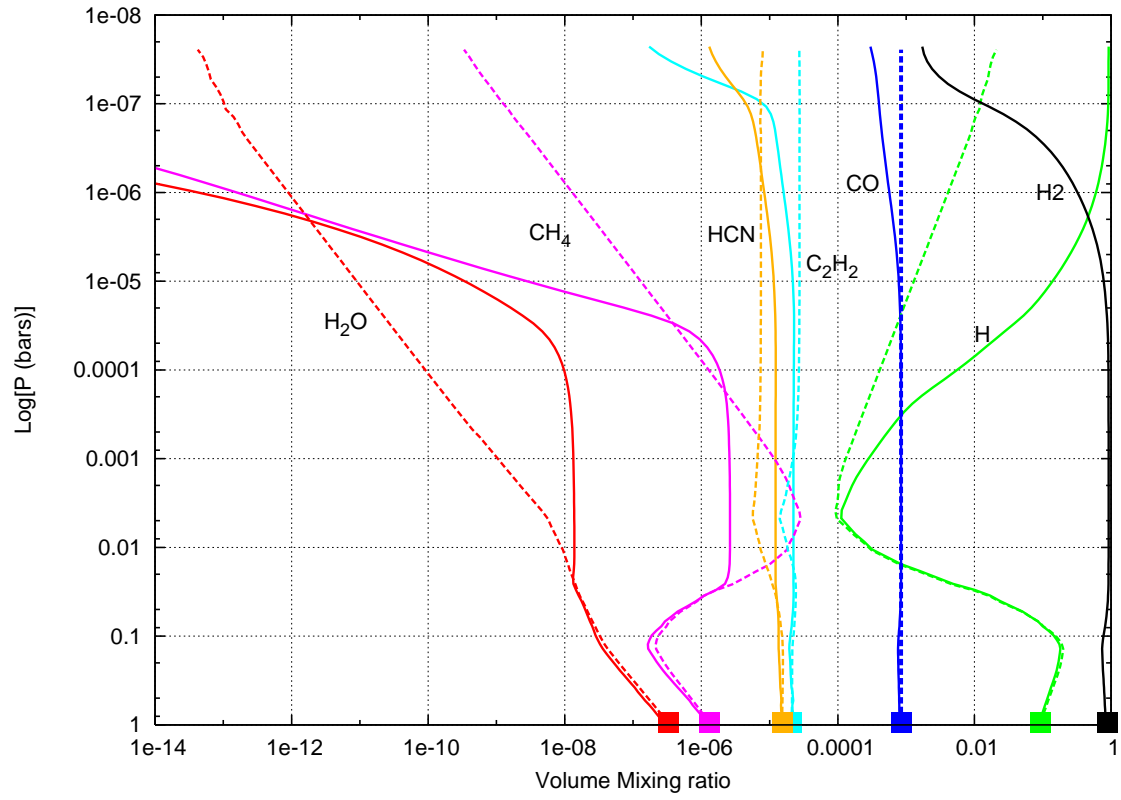


Fig. 4.— Mixing ratio profiles from equilibrium (dashed) and photochemical (solid) models for  $[C]/[O] = 1.08$  (twice solar)

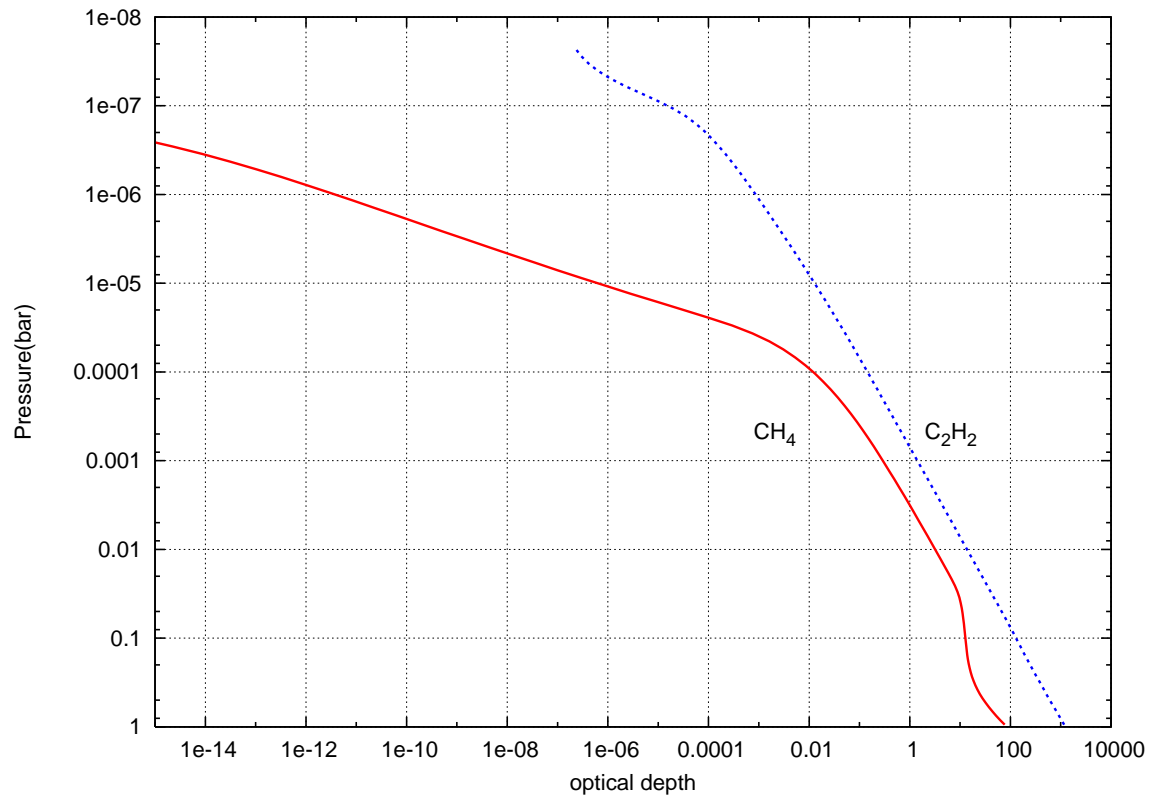


Fig. 5.— Approximate optical depths of the CH<sub>4</sub> 7.7 micron band (red solid) and the 7.5 micron  $\nu_2$  band (blue dashed) as a function of pressure. The optical depth of  $\nu_2$  is larger than CH<sub>4</sub> indicating that it may be the major absorber in WASP-12b's atmosphere.

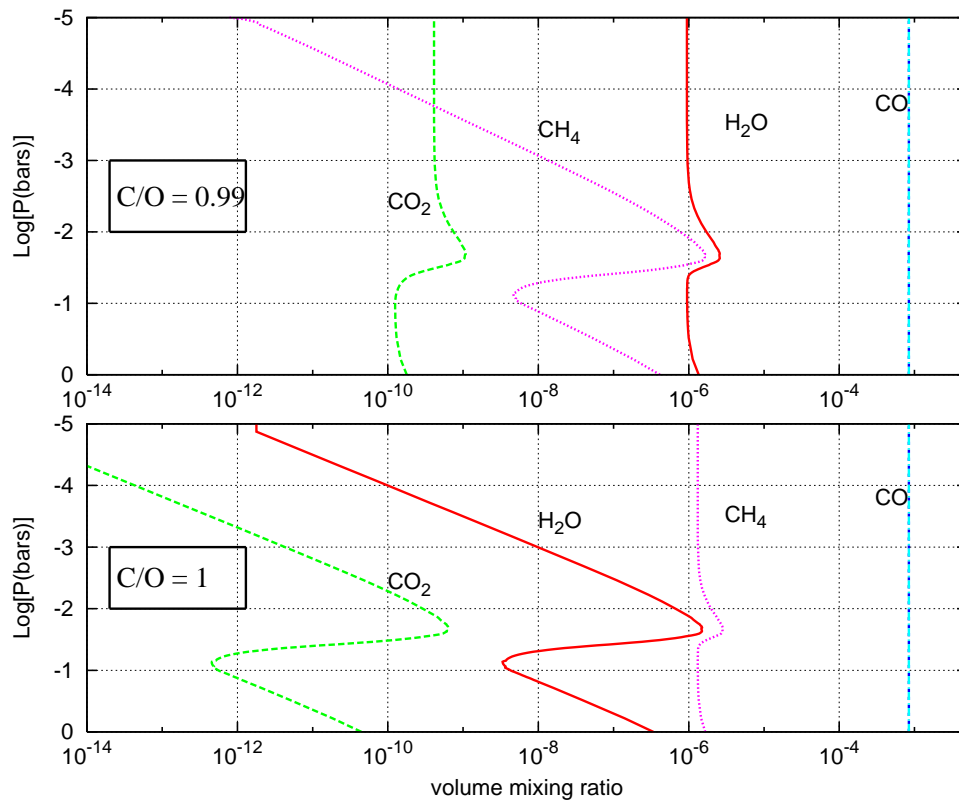


Fig. 6.— Diagrams showing the rapid shift in species' concentrations as C/O increases from 0.99 (top panel) to 1.0 (bottom panel).

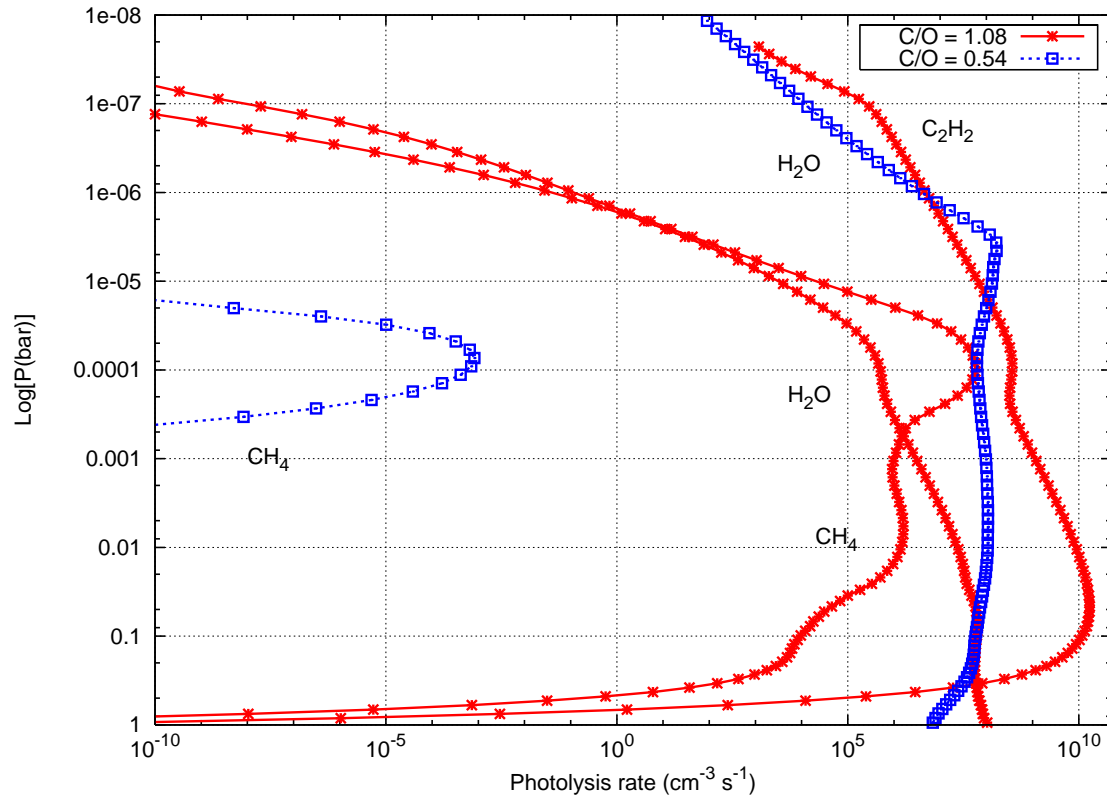


Fig. 7.— Photolysis rates of H<sub>2</sub>O and CH<sub>4</sub> for [C]/[O] = 0.54 (dashed, solar) and [C]/[O] = 1.08 (solid, super-solar) including  $\zeta h_2$ .



### A. Supplementary figures

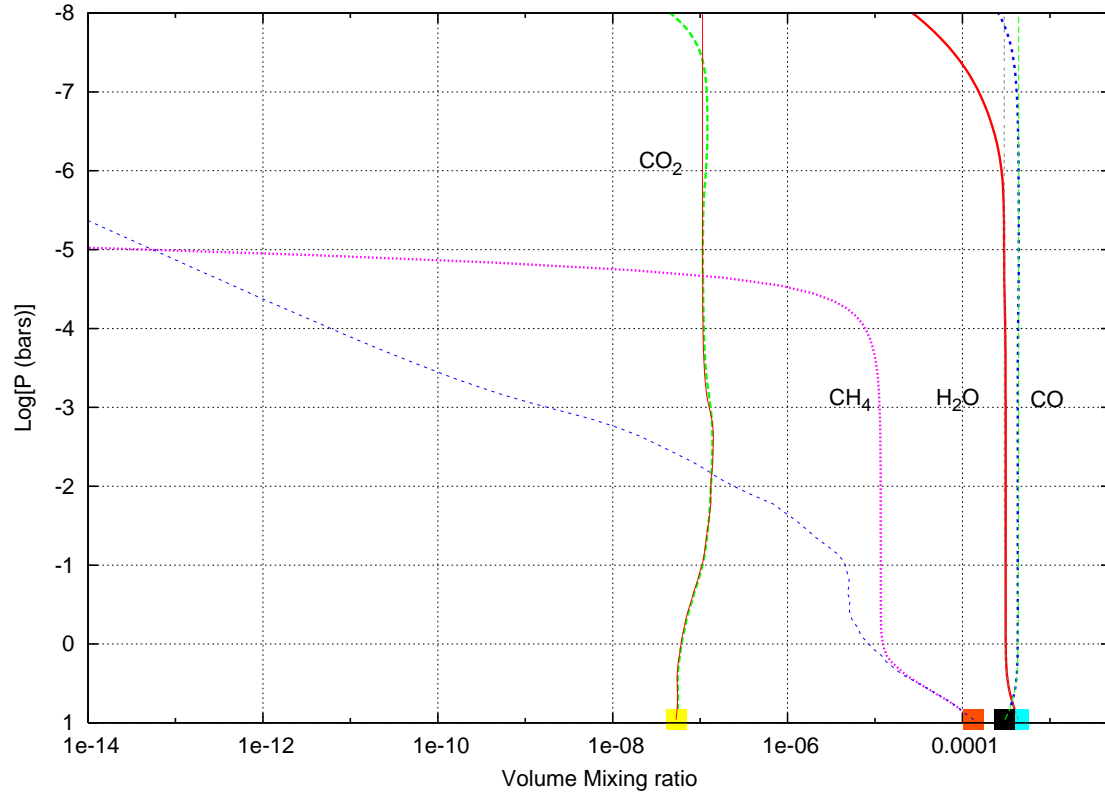


Fig. 8.— Photochemical mixing ratio profiles of H<sub>2</sub>O, CO, CH<sub>4</sub> and CO<sub>2</sub> derived from our model of the dayside atmosphere of HD 189733b. For comparison, see Line et al. (2010) and Moses et al. (2011).

Table 1. Reaction list and rate constants (Zahnle 2011) used in this study. Only the forward rate constants are given as we calculate reverse rate constants from the forward rate assuming thermodynamic equilibrium (see discussion in Section 2). For three body reactions, the first and second row represent the low and high pressure rate limits, respectively. A full version of the table is available in the electronic edition of the *Astrophysical Journal*.

Number	Reactants	Products	Rate <sup>a</sup>	Reference
1	H + H + M	→ H <sub>2</sub> + M	$8.8 \times 10^{-33}(T/298)^{-0.60}$	Baulch et al.(1992)
	H + H	→ H <sub>2</sub>	$1.0 \times 10^{-12}$	
2	O + H + M	→ OH + M	$4.3 \times 10^{-32}$	Tsang & Hampson (1986)
	O + H	→ OH	$1.0 \times 10^{-12}$	
3	H <sub>2</sub> + O	→ OH + H	$3.5 \times 10^{-13}(T/298)^{2.67}e^{-3160/T}$	Baulch et al.(1992)
4	H + OH + M	→ H <sub>2</sub> O + M	$6.6 \times 10^{-32}(T/298)^{-2.1}$	Javoy et al.(2003)
	H + OH	→ H <sub>2</sub> O	$2.7 \times 10^{-10}e^{-75/T}$	Cobos & Troe (1985)
5	H <sub>2</sub> + OH	→ H <sub>2</sub> O + H	$1.6 \times 10^{-12}(T/298)^{1.60}e^{-1660/T}$	Baulch et al.(1992)

<sup>a</sup>2-body reaction rates are in cm<sup>3</sup> s<sup>-1</sup>; 3-body rates are in cm<sup>6</sup> s<sup>-1</sup>.

